Thermal intravascular photoacoustic imaging

Bo Wang and Stanislav Emelianov*

Department of Biomedical Engineering, University of Texas at Austin, Austin, TX 78712, USA
**emelian@mail.utexas.edu*

Abstract: Intravascular photoacoustics (IVPA)—a minimally invasive imaging technique with contrast related to optical absorption properties of tissue, can be used to visualize atherosclerotic plaques. However, the amplitude of photoacoustic signals is also related to a temperature dependent, tissue specific parameter—the Grüneisen parameter. Therefore, photoacoustic signals measured at different temperatures may reveal information about tissue composition. In this study, thermal IVPA (tIVPA) imaging was introduced. The imaging studies were performed using an *ex vivo* atherosclerotic rabbit aorta. Temperature dependent photoacoustic responses from lipid in plaques and lipid in periadventitial tissue were different, thus allowing tIVPA images to delineate the location of lipid-rich plaques. The results indicate that tIVPA imaging has a potential to characterize tissue composition in atherosclerotic vessels.

OCIS codes: (110.5120) Photoacoustic imaging; (110.7170) Ultrasound; (170.0170) Medical optics and biotechnology; (170.6935) Tissue characterization

References and links

1. R. Virmani, A. P. Burke, A. Farb, and F. D. Kolodgie, "Pathology of the unstable plaque," Prog. Cardiovasc. Dis. **44**(5), 349–356 (2002).
2. D. Steinberg, "Thematic review series: the pathogenesis of atherosclerosis. An interpretive history of the cholesterol controversy: part I," J. Lipid Res. **45**(9), 1583–1593 (2004).
3. E. Falk, "Pathogenesis of atherosclerosis," J. Am. Coll. Cardiol. **47**(8 Suppl), C7–C12 (2006).
4. S. E. Nissen and P. Yock, "Intravascular ultrasound: novel pathophysiological insights and current clinical applications," Circulation **103**(4), 604–616 (2001).
5. C. L. de Korte, M. J. Sierevogel, F. Mastik, C. Strijder, J. A. Schaar, E. Velema, G. Pasterkamp, P. W. Serruys, and A. F. W. van der Steen, "Identification of atherosclerotic plaque components with intravascular ultrasound elastography *in vivo*: a Yucatan pig study," Circulation **105**(14), 1627–1630 (2002).
6. A. Nair, B. D. Kuban, E. M. Tuzcu, P. Schoenhagen, S. E. Nissen, and D. G. Vince, "Coronary plaque classification with intravascular ultrasound radiofrequency data analysis," Circulation **106**(17), 2200–2206 (2002).
7. Y. Shi, R. S. Witte, and M. O'Donnell, "Identification of vulnerable atherosclerotic plaque using IVUS-based thermal strain imaging," IEEE Trans. Ultrason. Ferroelectr. Freq. Control **52**(5), 844–850 (2005).
8. S. Sethuraman, S. R. Aglyamov, J. H. Amirian, R. W. Smalling, and S. Y. Emelianov, "Intravascular photoacoustic imaging using an IVUS imaging catheter," IEEE Trans. Ultrason. Ferroelectr. Freq. Control **54**(5), 978–986 (2007).
9. P. C. Beard and T. N. Mills, "Characterization of post mortem arterial tissue using time-resolved photoacoustic spectroscopy at 436, 461 and 532 nm," Phys. Med. Biol. **42**(1), 177–198 (1997).
10. Q. X. Chen, A. Davies, R. J. Dewhurst, and P. A. Payne, "Photo-acoustic probe for intra-arterial imaging and therapy," Electron. Lett. **29**(18), 1632–1633 (1993).
11. B. Wang, E. Yantsen, T. Larson, A. B. Karpiouk, S. Sethuraman, J. L. Su, K. Sokolov, and S. Y. Emelianov, "Plasmonic intravascular photoacoustic imaging for detection of macrophages in atherosclerotic plaques," Nano Lett. **9**(6), 2212–2217 (2009).
12. S. Sethuraman, J. H. Amirian, S. H. Litovsky, R. W. Smalling, and S. Y. Emelianov, "Spectroscopic intravascular photoacoustic imaging to differentiate atherosclerotic plaques," Opt. Express **16**(5), 3362–3367 (2008).
13. T. J. Allen and P. C. Beard, "Photoacoustic characterisation of vascular tissue at NIR wavelengths," Proc. SPIE **7177**, 71770A, 71770A-9 (2009).
14. B. Wang, J. L. Su, J. Amirian, S. H. Litovsky, R. Smalling, and S. Emelianov, "Detection of lipid in atherosclerotic vessels using ultrasound-guided spectroscopic intravascular photoacoustic imaging," Opt. Express **18**(5), 4889–4897 (2010).
15. K. Jansen, A. F. W. van der Steen, H. M. M. van Beusekom, J. W. Oosterhuis, and G. van Soest, "Intravascular photoacoustic imaging of human coronary atherosclerosis," Opt. Lett. **36**(5), 597–599 (2011).

#152125 - $15.00 USD Received 2 Aug 2011; revised 30 Sep 2011; accepted 3 Oct 2011; published 13 Oct 2011

16. J. M. Sun and B. S. Gerstman, "Photoacoustic generation for a spherical absorber with impedance mismatch with the surrounding media," Phys. Rev. E Stat. Phys. Plasmas Fluids Relat. Interdiscip. Topics **59**(5 Pt B), 5772–5789 (1999).
17. I. V. Larina, K. V. Larin, and R. O. Esenaliev, "Real-time optoacoustic monitoring of temperature in tissues," J. Phys. D Appl. Phys. **38**(15), 2633–2639 (2005).
18. J. Shah, S. Park, S. Aglyamov, T. Larson, L. Ma, K. Sokolov, K. Johnston, T. Milner, and S. Y. Emelianov, "Photoacoustic imaging and temperature measurement for photothermal cancer therapy," J. Biomed. Opt. **13**(3), 034024 (2008).
19. M. Shiomi and T. Ito, "The Watanabe heritable hyperlipidemic (WHHL) rabbit, its characteristics and history of development: a tribute to the late Dr. Yoshio Watanabe," Atherosclerosis **207**(1), 1–7 (2009).
20. T. Kobayashi, T. Ito, and M. Shiomi, "Roles of the WHHL rabbit in translational research on hypercholesterolemia and cardiovascular diseases," J. Biomed. Biotechnol. **2011**, 406473 (2011).
21. R. J. Havel, T. Kita, L. Kotite, J. P. Kane, R. L. Hamilton, J. L. Goldstein, and M. S. Brown, "Concentration and composition of lipoproteins in blood plasma of the WHHL rabbit. An animal model of human familial hypercholesterolemia," Arteriosclerosis **2**(6), 467–474 (1982).
22. C. L. Tsai, J. C. Chen, and W. J. Wang, "Near-infrared absorption property of biological soft tissue constituents," J. Med. Biol. Eng. **21**, 7–14 (2001).
23. D. E. Vance and J. E. Vance, *Biochemistry of Lipids, Lipoproteins, and Membranes*, New Comprehensive Biochemistry (Elsevier, 1996).
24. D. Vela, L. M. Buja, M. Madjid, A. Burke, M. Naghavi, J. T. Willerson, S. W. Casscells, and S. Litovsky, "The role of periadventitial fat in atherosclerosis," Arch. Pathol. Lab. Med. **131**(3), 481–487 (2007).

1. Introduction

Rupture of atherosclerotic plaques leads to many life-threatening cardiovascular events. Rupture-prone plaques may be identified based on their composition. For example, a plaque with a large lipid pool covered by a thin, macrophage-infiltrated fibrous cap has a high likelihood to rupture [1]. Lipid is one of the most important components in atherosclerotic plaques. Lipid in plaques results from accumulation of low density lipoprotein (LDL) particles infiltrated into the arterial wall from vessel lumen. At the early stage of atherosclerosis, fatty streaks can be observed from the vessel lumen [2]. As the disease progresses, lipid deposits contribute to the soft, destabilizing necrotic core inside the plaques. The location and the size of the necrotic lipid core are critical for the analysis of plaque stability [3].

Many imaging modalities are dedicated to detecting rupture-prone plaques by characterizing tissue composition. Among these, intravascular imaging modalities generally provide high-resolution, real-time images of the vessel wall, which lead to better disease diagnosis and assist in the guidance of interventional therapeutic procedures. Intravascular ultrasound (IVUS) imaging is the most widely used minimally invasive modality for imaging the anatomy of the vessel wall. Lipid-rich plaques appear hypo-echoic in IVUS images [4]. Because of limited contrast between lipid-rich regions and other tissue types, additional approaches are deployed for better distinction of lipid-rich plaques. For example, by analyzing the displacement and strain maps within the vessel wall during the cardiac cycle, intravascular elastography can differentiate fatty versus fibrous plaques based on the tissue strain [5]. Through analyzing the radiofrequency acoustic signal in the frequency domain, plaque composition can be classified into fibrous, fibrolipidic, calcified, and calcified-nectronic plaques [6]. Furthermore, as temperature increases, the speed of sound decreases in the fat while increases in water—based on such contrast, IVUS based thermal strain imaging can also be used to detect lipid rich plaques [7].

Ultrasound-guided intravascular photoacoustic (IVPA) imaging is a minimally invasive imaging modality for imaging atherosclerosis [8]. IVPA imaging is sensitive to optical absorption contrast inside the vessel wall [9,10]. By combining an IVPA image with its co-registered IVUS image, the distribution of the endogenous and exogenous optical absorption contrast inside the vessel wall can be visualized [8,11]. IVPA imaging has the potential to characterize plaque composition based on the characteristic optical absorption spectra of various tissue types [12]. Spectroscopic IVPA imaging at optical wavelengths near 1210 nm has been used to detect lipid-rich plaques in an *ex vivo* atherosclerotic animal and human arteries [13–15]. Here we demonstrate that thermal properties of the tissues can be used to generate contrast in IVPA images and distinguish between the plaque and other vascular tissues.

#152125 - $15.00 USD Received 2 Aug 2011; revised 30 Sep 2011; accepted 3 Oct 2011; published 13 Oct 2011

In IVPA imaging, the vessel wall is irradiated by a short laser pulse. Tissue then undergoes thermal expansion upon absorbing laser energy and subsequently generates photoacoustic (PA) waves. If the laser pulse duration is significantly shorter than the thermal and stress relaxation time of the tissue, the heat generated by optical absorption does not have time to diffuse out of the heated region during the laser pulse. The maximum initial PA pressure p_0 then has the following form [16]:

$$p_0 = \frac{v_s^2 \beta}{C_p} \mu_a F e^{-\mu_{eff} z}, \tag{1}$$

where μ_a is the optical absorption coefficient of the tissue; F is the laser fluence; μ_{eff} is the effective attenuation coefficient of light in tissue; z is the depth, and Γ is the Grüneisen parameter defined as

$$\Gamma = \frac{v_s^2 \beta}{C_p}, \tag{2}$$

where v_s denotes the speed of sound; β is the thermal coefficient of volume expansion; C_p is the specific heat capacity at constant pressure. Because v_s, β, and C_p are all temperature-dependent, tissue-specific parameters, so is the Grüneisen parameter Γ. Therefore, if the Grüneisen parameter of a specific tissue type at various temperatures is known, PA imaging can be used to remotely monitor the temperature change [17,18]. Alternatively, tissue composition may be identified based on temperature-dependent PA responses. In this study, by changing the temperature, lipid-rich plaques are detected based on their characteristic temperature-dependent IVPA signal change. This technique is thus referred to as thermal IVPA (tIVPA) imaging.

2. Materials and methods

2.1. Animal model

A Watanabe heritable hyperlipidemic (WHHL) rabbit was used as the animal model for atherosclerosis. WHHL rabbits have high LDL levels in circulating blood due to their genetic deficiency of LDL receptors. This type of rabbit can spontaneously develop atherosclerosis in the aorta and coronary arteries [19]. Lipid metabolism and atherosclerotic plaques of WHHL rabbit resemble that of human [20,21]. Within 12 to 18 months of age, severe plaques build up in the arteries of WHHL rabbits.

In this study, the abdominal aorta procured from a one year old WHHL rabbit was used for tIVPA imaging. Prior to imaging, a WHHL rabbit was sacrificed and the segment of the aorta was removed and preserved in saline damped gauze at around 4°C. Imaging experiments were performed within 24 hours after sacrificing the rabbit.

2.2. Imaging system

To image an excised vessel, a bench top, combined intravascular IVUS/IVPA imaging system was used (Fig. 1). The *ex vivo* aorta sample was immersed inside a water cuvette filled with saline. A 40 MHz single element IVUS imaging catheter (Boston Scientific, Inc.) was placed inside the vessel lumen. The transducer located at the tip of the imaging catheter was aligned with the optical fiber. The aorta sample was rotated by a stepper motor (Zaber, Inc.) for cross-sectional scanning. Each cross-sectional scanning consisted of 256 A-lines. The laser source for IVPA imaging was provided by a tunable optical parametric oscillator (OPO) laser system (Spectra-Physics, Inc.) capable of generating laser pulses of approximately 3-5 ns duration at 10 Hz repetition rate. The energy of each laser pulse was recorded for off-line compensation of the pulse-to-pulse laser energy variation. Once a laser pulse was generated, an analog to digital convertor card (CompuScope 14200, GaGe, Inc.) was triggered to sample the radio frequency signal at a 200 MHz sampling rate. After a user defined delay, a pulser/receiver

#152125 - $15.00 USD Received 2 Aug 2011; revised 30 Sep 2011; accepted 3 Oct 2011; published 13 Oct 2011

(5073PR, Olympus, Inc.) was triggered for conventional intravascular ultrasound imaging. The system was capable of acquiring co-registered IVPA and IVUS images of the aorta sample in a cross-sectional view.

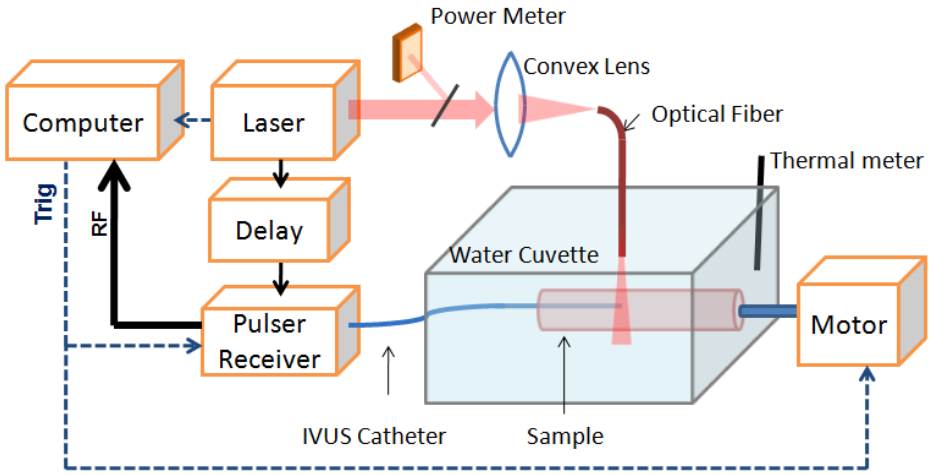

Fig. 1. Combined IVUS/IVPA imaging system for tIVPA imaging.

2.3 Experimental protocol

The abdominal aorta sample was imaged *ex vivo* within 24 hours after sacrificing the WHHL rabbit. During the imaging experiment, the aorta sample was placed inside the water cuvette with one end attached to a fixture connected to the stepper motor (Fig. 1). The temperature of the aorta sample was changed by adding warm saline, and then cooled down with ice. In order to confirm that the temperature-dependent PA responses were consistent and reversible, the increase and decrease in temperature was repeated three times. Tissue temperature was monitored by a digital thermometer placed inside the water cuvette.

2.4 Image processing

IVPA images acquired at two different temperatures were spatially averaged with a kernel size of 266 μm (axial) by 15.5 degree (azimuthal). The kernel size was around five times larger than the axial resolution and two times larger than the azimuthal resolution of IVPA imaging. The relatively large size of the kernel was selected to minimize the effect of the unwanted tissue motion caused by several factors including irregular mechanical rotation of the sample as well as addition of ice or warm saline to the water cuvette. Then, the finite difference of the PA amplitude between the two IVPA images was calculated as

$$D_{i,j} = \frac{S_{i,j}^{T_2} - S_{i,j}^{T_1}}{(T_1 - T_2) \cdot S_{i,j}^{T_1}}, \tag{3}$$

where $S_{i,j}^{T}$ is the PA signal amplitude at pixel i, j at temperature T, and $D_{i,j}$ is the resultant finite difference map. The finite difference map was then color-coded to form the tIVPA image, and displayed over the co-registered IVUS image to show the relative location and magnitude of the tIVPA signal in context of vessel morphology.

3. Results

The rabbit aorta was imaged first at room temperature (25°C) using combined IVUS/IVPA imaging system. IVPA imaging was performed at 1210 nm wavelength because lipid has a high optical absorption coefficient at this wavelength [22]. The cross-sectional IVUS image of the vessel showed two hypo-echoic regions that corresponded to the location of plaques

#152125 - $15.00 USD Received 2 Aug 2011; revised 30 Sep 2011; accepted 3 Oct 2011; published 13 Oct 2011

(yellow arrows in Fig. 2(a)). The combined IVUS/IVPA image of the same cross-section is presented in Fig. 2(b). Strong PA signals present at the plaque region indicated that these plaques were rich in lipid. Strong PA signals were also observed at the periadventitial regions of the aorta. These signals may have originated from the periadventitial fat due to high optical absorption, high surface optical fluence, and subsurface optical fluence due to the refractive index mismatch between saline and arterial tissue. Oil red O stain for lipid, performed on the tissue section adjacent to the imaged cross-section, confirmed that the aorta contained lipid rich plaques in the intimal layer (Fig. 2(c)).

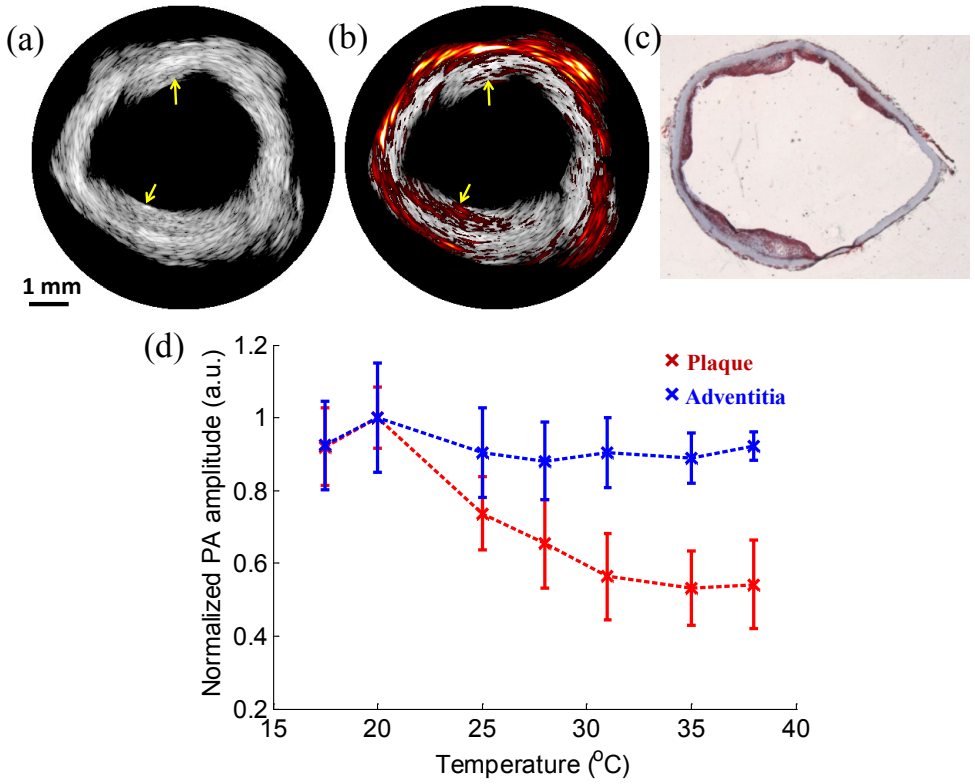

Fig. 2. (a) IVUS and (b) combined IVUS/IVPA (1210 nm wavelength) images of the atherosclerotic vessel. The images were acquired at 25°C. Yellow arrows in these images indicate the location of atherosclerotic plaques. (c) Oil red O stain confirmed that the imaged aorta had lipid-rich plaques. The angular position of the histological slide was chosen based on the visual correlation of the shape of the vessel wall in histology and the IVUS image. (d) Comparison of the temperature dependent normalized amplitude of PA signal in plaque and the adventitia (error bars correspond to plus/minus one standard deviation).

To observe the temperature dependent PA response, the temperature of the artery was changed from 38 °C to 17.5 °C three times, and PA responses from areas with high PA signal were analyzed. Specifically, four regions within the plaque and the periadventitial sections were identified and PA signals within these regions were averaged. The amplitude of PA signal was then normalized to the maximum amplitude and plotted versus temperature (Fig. 2(d)). Interestingly, the PA amplitude from periadventitial regions does not change and remained relatively constant with temperature, while the PA amplitude from plaques decreased with increasing temperature. The different trends of the PA amplitude demonstrates that the Grüneisen parameters for lipid in plaques and tissues in the periadventitial region have different temperature dependencies and, therefore, suggests that lipid in plaques may be differentiated based on the tIVPA imaging.

#152125 - $15.00 USD Received 2 Aug 2011; revised 30 Sep 2011; accepted 3 Oct 2011; published 13 Oct 2011

Using IVPA data obtained at 25 °C and 38 °C, a finite difference map was calculated based on Eq. (3) and a tIVPA image was generated. The regions with decreasing PA amplitude versus temperature ($0.4/13 < D_{i,j} < 0.95/13$) were colored orange, and displayed over the co-registered IVUS image (Fig. 3(a)). As shown in the tIVPA image (Fig. 3(a)), the PA responses from plaque regions showed consistently decreasing PA amplitude with increasing temperature, while the PA response from the periadventitial regions was different.

Spectroscopic IVPA (sIVPA) imaging at the same cross-section of the aorta was performed within 1210-1230 nm wavelength range [14]. Similar to tIVPA imaging, sIVPA imaging of lipid also successfully delineated lipid-rich regions in the arterial wall (Fig. 3 (b)), confirming that lipid regions in the tIVPA image reflected lipid deposits inside the plaque. Interestingly, compared to the tIVPA image, sIVPA image showed more lipid constituents in the periadventitial layer of the aorta. This difference indicates that although the lipid deposits in plaques and the periadventitial fat have similar optical properties, their Gruneisen parameter and, therefore, temperature dependent PA response are different.

To further investigate the differences of temperature dependent PA responses between lipid in plaques and lipid in adipose tissue, a sample of rabbit abdominal fat was imaged with the combined IVUS/IVPA imaging system (Fig. 1) by placing the tissue sample between the

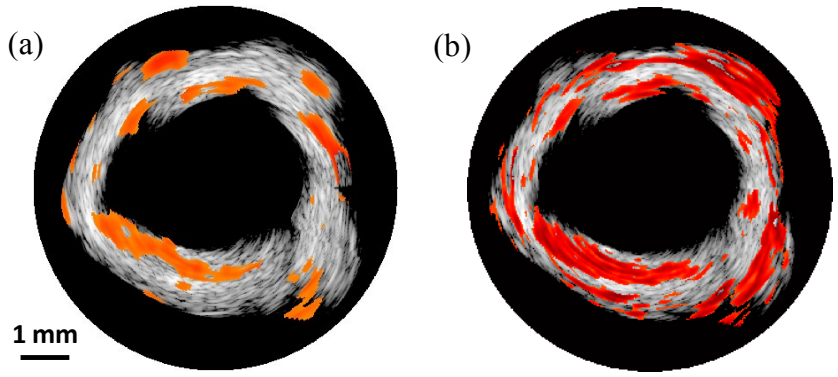

Fig. 3. (a) Thermal IVPA (tIVPA) and (b) spectroscopic IVPA (sIVPA) images of the same cross-section of the atherosclerotic artery. Lipid-rich atherosclerotic plaques have similar appearance in tIVPA and sIVPA images while periadventitial fat does not appear in the tIVPA image.

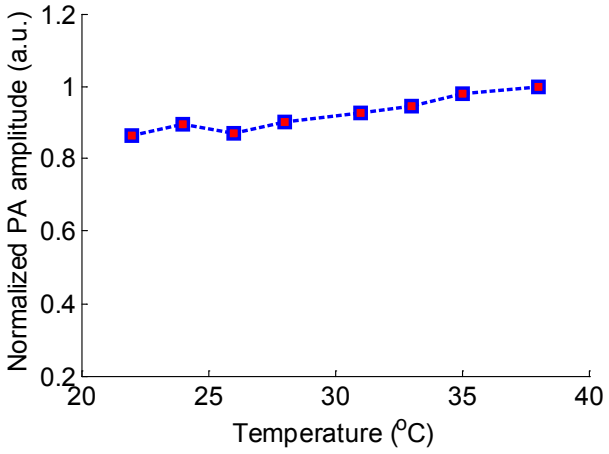

Fig. 4. Temperature dependence of the normalized amplitude of PA signal measured in a sample of rabbit's abdominal fat.

#152125 - $15.00 USD Received 2 Aug 2011; revised 30 Sep 2011; accepted 3 Oct 2011; published 13 Oct 2011

optical fiber and the single element IVUS catheter. PA signals were acquired at various temperatures at 1210 nm wavelength and normalized to the maximum of the amplitude of PA signal. As shown in Fig. 4, the PA amplitude increases slightly within 22°C to 38°C temperature range. Such a trend is opposite to the temperature dependence of the PA signal generated by lipid deposits in the plaques (Fig. 2(d), red line), therefore confirming that adipose tissue has a different temperature dependent PA response compared to lipid in plaques.

4. Discussion and conclusions

We demonstrated that tIVPA imaging can be used to differentiate tissues, in particular, lipid in atherosclerotic plaques and adipose tissue. With increasing tissue temperature, the PA amplitude of lipid in plaques decreased while the PA amplitude of lipid in periadventitial and abdominal fat remained relatively constant within 20–38°C temperature range. The different trends of the PA responses indicated that the Grüneisen parameter of lipids from various regions of body have unique temperature dependences. These dependences may result from differences in tissue composition. Adipose tissues mainly consist of triglyceride, whereas lipid deposits in atherosclerotic plaques originate from LDL particles having a low triglyceride concentration, but a high concentration of cholesterol and cholesterol esters [23]. The difference in triglyceride concentration may be the source of tIVPA contrast.

Various factors such as depth- and wavelength-dependent fluence distribution, the small displacement of aorta sample between different cross-sectional scans, and the variability in acoustic pressure and the sensitivity of the IVUS imaging catheter can influence the amplitude of the PA signal. However, these factors do not affect significantly the temperature dependence of the PA response and, therefore, the contrast in tIVPA images.

The difference of thermal PA responses between lipid in plaques and adipose tissue was studied using a rabbit model of atherosclerosis. In humans, the change of PA signal with temperature (Fig. 3(d)) may be different because human lipoprotein particles contain different proportion of lipid component [21]. Therefore, future studies using human atherosclerotic tissue needs to be performed to identify the proper temperature range for the detection of lipid-rich plaques. tIVPA imaging can also be used to detect periadventitial fat in atherosclerotic vessels, which relates to the progression of atherosclerosis [24].

In clinical practice, the decrease or increase of the temperature of the blood vessel wall may be induced by flushing low temperature fluid, inflating a balloon catheter filled with low temperature fluid, or irradiating the artery wall with ultrasound wave or electromagnetic radiation (e.g. laser light or microwaves). Thermal PA imaging of lipid can also be applied to image superficial vessels such as carotid arteries. Finally, thermal PA imaging may also be applied to cancer diagnosis and imaging of other pathologies where lipid plays an important role in disease formation and progression.

In conclusion, IVPA imaging was performed *ex vivo* on an atherosclerotic rabbit artery at different temperatures. Different temperature dependencies of PA responses were found in lipid and periadventitial fat. Based on the thermal PA responses, we introduced thermal intravascular photoacoustic (tIVPA) imaging to differentiate lipid in atherosclerotic plaques. The advantage of tIVPA imaging is that it could be performed using an IVPA imaging system operating at a single wavelength. More importantly, tIVPA imaging has the potential to differentiate lipids that have the same optical absorption property and, therefore, may not be distinguishable using conventional photoacoustic imaging approaches.

Acknowledgments

This work was supported in part by the National Institutes of Health under grant HL096981. Tissue samples were provided by Dr. Richard Smalling and Mr. James Amirian from the University of Texas Health Science Center in Houston. The authors would like to thank Dr. Wolfgang Frey from the Department of Biomedical Engineering at the University of Texas at Austin for helpful discussions. The authors would also like to acknowledge the technical support from Boston Scientific, Inc.

#152125 - $15.00 USD Received 2 Aug 2011; revised 30 Sep 2011; accepted 3 Oct 2011; published 13 Oct 2011